Ab initio adiabatic He and Ne interaction on Ag: An all-electron calculation

M. I. Trioni, S. Marcotulio, G. Santoro, and V. Bortolani
Istituto Nazionale di Fisica della Materia and Dipartimento di Fisica, Università di Modena, via Campi 213/A, 41100 Modena, Italy

G. Palumbo and G. P. Brivio
Istituto Nazionale di Fisica della Materia and Dipartimento di Scienza dei Materiali, Università di Milano, via Emanueli 15, 20126 Milano, Italy

(Received 6 April 1998)

We report an *ab initio* calculation of the adiabatic electronic properties of He and Ne atoms interacting with an Ag-like jellium metal surface, using the embedding method and the density functional theory in the local density approximation (LDA). Differently from previous results obtained in this framework, the noble atoms are described with their full potential. The linearized augmented plane-wave basis set is introduced to tackle the Kohn-Sham equation. Attention is focused on the atom-surface potential in the repulsive regime, i.e., at distances from the jellium edge smaller then the adsorption one, where the LDA has been shown to work well, and which are relevant in elastic and inelastic scattering experiments of He and Ne on metals. For incident atoms with initial kinetic energies in the experimental range of interest, it is shown that Ne gets closer to the metal than He as previously found with an Al substrate. An analysis of the shift of the atomic core levels by varying the atom-metal distance is also presented. [S0163-1829(98)01539-2]

I. INTRODUCTION

The main goal of physisorption theory of noble gases on metals is to obtain the particle-surface interaction in a unified approach valid at any atom distance from the surface. In principle this could be obtained within the density functional theory (DFT). In practice, the usual difficulty that one has to tackle when writing down such a unified theory, is to obtain the nonlocal response function of the metal. In this respect, a recent attempt has been performed via a local approximation of the dielectric function of the metal by Hult *et al.*[1] But this is still an open and important question because the correct van der Waals behavior of the gas-metal potential affects both the amplitudes of light noble gas probes scattering off metals[2] and dynamical quantities such as sticking coefficients and desorption rates.[3] To overcome this problem, various approaches have been proposed.[4–8] In the field of *ab initio* methods, one usually calculates the physisorption potential closer to the surface of a noble-gas atom interacting with a metal surface and add subsequently the van der Waals part.[9,10] Note that, to obtain a minimum in the physisorption potential, the van der Waals interaction has to be added if the approach is only capable of obtaining the repulsive part.[11] Alternatively, in some other approaches, such as DFT using the local density approximation (LDA), a reasonable physisorption well can be obtained,[12,13] although the calculated potential does not display the correct van der Waals tail, namely, it drops to zero exponentially. This is because the LDA accounts well for a phenomenon such as the Pauli repulsion experienced by a noble gas atom very close to the metal. In addition, regarding the atom-metal equilibrium distance, Lang,[12] in his work on jellium, has shown that the LDA may provide a good account of the adatom binding energy. An intuitive explanation of this effect is related to the fact that, at such atom-surface distances, it is correct to consider the electron to be attached to its exchange-correlation hole as in the LDA.

The results presented in this paper are determined within the embedding method for an isolated adsorbate in the framework introduced in Ref. 14. In this method, the Schrödinger equation, in the DFT-LDA framework, is solved in a localized region embedded within an extended system. In the present problem the localized region contains the He or Ne atom plus that region of the surface significantly perturbed by the adatom, while the extended system is the remainder of a semi-infinite substrate. Such a framework has two main properties valid for any molecule-surface system: (i) the adsorbate is really isolated; i.e., there is no two-dimensional periodicity of the adsorbate system, and (ii) the substrate is infinitely extended.[15] In this way we avoid adsorbate-adsorbate interactions to be found in slab-supercell calculations and also we take into account the continuum electronic states of substrate. For such reasons, an *ab initio* description of the isolated chemical species on a semi-infinite solid can provide more accurate information on the particle-surface adiabatic interaction. In the embedding approach, the influence of the extended substrate enters in the form of a nonlocal energy-dependent potential, added to the Hamiltonian, which acts upon the surface enclosing the embedded volume. We determine this embedding potential from the Green function of the substrate in the absence of the adsorbate. Eventually all the relevant physical quantities are obtained as in other methods by projecting our equation onto a suitable basis set. However, unlike methods based upon the Dyson equation, our boundary conditions do not enter as an expansion throughout the embedded volume, giving us more flexibility for the choice of the basis set. In addition, our method is based upon a variational solution of the Schrödinger equation, without any *a priori* biasing in the behavior of the Green function.

However, we observe that the embedding method may not be the most effective one for determining the adiabatic electronic properties of a noble-gas–atom–metal system. This is because the electronic states do not lie within the metal band as occurs for chemisorbed atoms and/or molecules, so that the continuous character of the local density of states here is not crucial. But just because of this reason, an *ab initio* calculation of the electronic properties of a noble gas on a metal could show that the embedding approach is flexible enough to be applied to a variety of adsorbate systems.

A limitation to be found in our results (not of the embedding method) is the use of a jellium substrate instead of one with a lattice structure. In this paper we shall present results on the adiabatic noble-gas–surface interaction for a metal system with an intermediate electron density with $r_s^{\mathrm{Ag}} = 3.02a_0$.[16] This often refers to an Ag substrate though we are aware that in our calculation we do not include all the physical properties following from the substrate periodicity. However, we expect our results to be still interesting both to describe the adiabatic interaction of He and Ne on an Ag substrate and to compare them with previous ones on a higher density Al-like jellium ($r_s^{\mathrm{Al}} = 2.07a_0$). We also remark that several results for physisorbed atoms on metals have been obtained in the framework of this simplification for the surface,[10,12,13,17] while recent *ab initio* calculations,[18] incorporating a realistic metal surface, have not addressed in detail the question of the penetration depth of He and Ne.[19,20]

In the following section we shall present a derivation of the main equations of our method, and discuss their solution. In particular, the linearized augmented plane-wave expansion in the embedding approach is outlined. Section III illustrates the application of the method to the isolated noble gas interacting with the surface of Ag modeled as jellium. Section IV is devoted to conclusions.

II. THE EMBEDDING APPROACH

A. Outline

The embedding method[14,21–23] has been developed for the study of extended systems where a localized perturbation has lowered the symmetry and has caused a significant enhancement of the complexity. There are many examples of these locally broken symmetries: impurities within a bulk crystal, interfaces in general and surfaces in particular, adsorbates at surfaces, and so on.

Embedding exploits the fact that very often in these systems the electronic charge density is significantly perturbed only within a limited region. In fact, for example, in a metal, the electrons rearrange themself at short distances from the impurity, screening efficiently the perturbation. From the knowledge of the charge density, in principle, all the ground-state properties may be determined.[24] In the present context this means quantities of interest such as the adsorption energy, the density of states or the band structure (spectrum), the bonding site and geometry of the adsorbate, and the potential energy surfaces for surface processes such as dissociation or diffusion.[3]

Since the disturbance is essentially localized, it makes sense to see whether one can obtain the perturbed charge density from a calculation that only considers a limited region around the impurity. So the embedding approach concentrates effort and resources on the region where the important physics is going on. The difficulty is, of course, that there is coupling to the extended (unperturbed in the first approximation) system, and that this coupling is important, for example, for broadening localized levels into resonances, and providing a source of electrons that can then freely flow into and out of the perturbed region. This last phenomenon is typical of any calculation in which the Fermi energy is pinned at the unperturbed system value. In this framework the total charge is no longer conserved not only in the localized region, but also in the whole space and a grand-canonical Hamiltonian has to be considered to determine the total energies.[25]

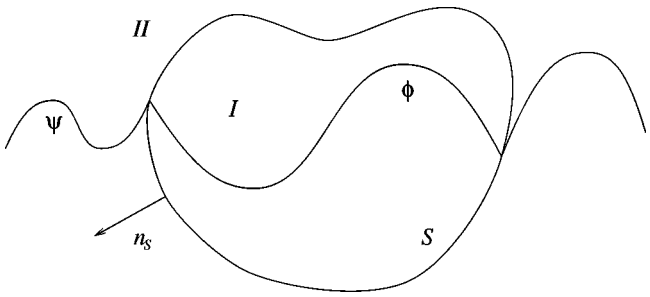

FIG. 1. The embedding geometry, with region I to be embedded in the extended region II.

In the embedding approach the extended system may be taken into account if the localized region is considered with the appropriate boundary condition. This boundary condition will influence the solution of the Schrödinger equation found within the smaller region. Since the region beyond the smaller volume remains unperturbed, the boundary condition will not depend upon the perturbation. In the embedding method, the boundary condition is implemented via a nonlocal, energy-dependent potential that acts upon the dividing surface of the two regions. Such an embedding potential is derived from a calculation performed on the unperturbed system once, and independently of which impurity is considered.

We briefly summarize the derivation of the embedding equations, highlighting pertinent points. Further details and discussion are to be found in Refs. 21,22. The total space is partitioned into regions I and II (Fig. 1). The former is the volume to be embedded, the region that contains the admolecule and that part of the system perturbed by its presence. Region II is the rest of the extended system, containing the substrate. A *variational* solution to the single-particle Schrödinger equation may be found that explicitly depends only upon the wave function in region I, the region of interest. To do this we construct a trial wave function $\phi(\boldsymbol{r})$, which is to be varied within region I and which in region II is a solution $\psi(\boldsymbol{r})$ of the Schrödinger equation for the unperturbed system at energy ε. On the surface S, which divides the two volumes I and II, the trial wave function is continuous, $\phi(\boldsymbol{r}_S) = \psi(\boldsymbol{r}_S)$, as it must be to be a valid wave function, but a discontinuity in derivative is permitted.

The expectation value of the Hamiltonian H in the whole space is given by

$$E=\frac{\int_{\mathrm{I}} d^3\boldsymbol{r}\phi^* H\phi+\varepsilon\int_{\mathrm{II}} d^3\boldsymbol{r}|\psi|^2+\frac{1}{2}\int_S d^2\boldsymbol{r}_S\phi^*(\partial\phi/\partial n_S-\partial\psi/\partial n_S)}{\int_{\mathrm{I}} d^3\boldsymbol{r}|\phi|^2+\int_{\mathrm{II}} d^3\boldsymbol{r}|\psi|^2}, \tag{1}$$

where n_S is the unit vector normal to the infinitesimal surface elements $d^2\boldsymbol{r}_S$ pointing out of the region I, and the surface integral term is the kinetic energy contribution arising from the discontinuity of the wave function derivative across S. The volume integral in region I may be eliminated by introducing the Green function G_0 for the unperturbed system, which satisfies a zero normal-derivative boundary condition on S:

$$\frac{\partial G_0(\boldsymbol{r}_S,\boldsymbol{r}';\varepsilon)}{\partial n_S}=0. \tag{2}$$

The surface inverse $G_0^{-1}(\boldsymbol{r}_S,\boldsymbol{r}_S';\varepsilon)$ of this Green function, defined by

$$\int_S d^2\boldsymbol{r}_S' G_0^{-1}(\boldsymbol{r}_S,\boldsymbol{r}_S';\varepsilon)G_0(\boldsymbol{r}_S',\boldsymbol{r}_S'';\varepsilon)=\delta(\boldsymbol{r}_S-\boldsymbol{r}_S''), \tag{3}$$

is a generalized logarithmic derivative that relates the amplitude and derivative of the wave function on surface S:

$$\frac{\partial\psi(\boldsymbol{r}_S)}{\partial n_S}=-2\int_S d^2\boldsymbol{r}_S' G_0^{-1}(\boldsymbol{r}_S,\boldsymbol{r}_S';\varepsilon)\psi(\boldsymbol{r}_S'). \tag{4}$$

Following Ref. 21 we can thus obtain the expectation value of the Hamiltonian with our trial function, purely in terms of quantities evaluated within or on the surface of region I:

$$E=\frac{\int_{\mathrm{I}} d^3\boldsymbol{r}\phi^* H\phi+\frac{1}{2}\int_S d^2\boldsymbol{r}_S\phi^*\partial\phi/\partial n_S+\int_S d^2\boldsymbol{r}_S\int_S d^2\boldsymbol{r}_S'\phi^*(G_0^{-1}(\varepsilon)-\varepsilon\partial G_0^{-1}(\varepsilon)/\partial\varepsilon)\phi}{\int_{\mathrm{I}} d^3\boldsymbol{r}|\phi|^2-\int_S d^2\boldsymbol{r}_S\int_S d^2\boldsymbol{r}_S'\phi^*\partial G_0^{-1}(\varepsilon)/\partial\varepsilon\,\phi}. \tag{5}$$

If this equation is minimized with respect to the trial function ϕ, we obtain the following Schrödinger equation:

$$\left(H+\frac{1}{2}\delta(\boldsymbol{r}-\boldsymbol{r}_S)\frac{\partial}{\partial n_S}\right)\phi(\boldsymbol{r})+\delta(\boldsymbol{r}-\boldsymbol{r}_S)\int_S d^2\boldsymbol{r}_S'\left(G_0^{-1}(\boldsymbol{r}_S,\boldsymbol{r}_S';\varepsilon)+(E-\varepsilon)\frac{\partial G_0^{-1}(\boldsymbol{r}_S,\boldsymbol{r}_S';\varepsilon)}{\partial\varepsilon}\right)\phi(\boldsymbol{r}_S')=E\phi(\boldsymbol{r}),\quad \text{with } \boldsymbol{r}\in I. \tag{6}$$

We consider each term in turn: H is the Hamiltonian of the system, a sum of kinetic energy and potential energy operators. The normal derivative term on the embedding surface provides Hermiticity within region I. G_0^{-1} is the embedding potential, constraining the trial function ϕ to correctly match onto the substrate wave functions ψ. The energy-derivative term provides a first-order correction to G_0^{-1}, so that the constraint is evaluated at the working energy E. The correction vanishes if G_0^{-1} is evaluated at energy E, as is done in practice for a continuous spectrum. Further details about the minimization procedure involving the parameter ε are to be found in Ref. 21.

The embedding potential contains all the information regarding the substrate that will enter into the solution of the Schrödinger equation for the perturbed region. It does not depend upon the contents of the embedded volume, and need to be evaluated only once for a given substrate and choice of embedding volume. Hence it is worthwhile to evaluate it to high accuracy. Once this has been done an arbitrary perturbation may be introduced into the embedded region, and the electronic structure is obtained from a calculation for this region with the embedding potential acting as a boundary condition. Such a solution will be entirely equivalent to having solved the problem of the combined substrate+adsorbate system *assuming complete basis set convergence and that the perturbation in the charge density and potential are restricted to the embedded volume.*

B. Matrix representation

In the previous section the trial wave function that minimizes the expectation value of the Hamiltonian was shown to satisfy an effective Schrödinger equation. To achieve this minimization in practice, we expand the trial wave function in a basis set and minimize with respect to the expansion coefficients, obtaining a matrix-equation representation of the Schrödinger equation. We find it convenient to solve Eq. (6) in terms of its Green function G. There are beneficial reasons for switching from the electronic wave function to the single-particle Green function. The analyticity of the Green function may be exploited to simplify valence integration through the use of complex energies, and a better description for the spectral features and the local density of states is obtained. However, the presence of the energy-dependent embedding potential in Eq. (6), prevents the solu-

tion from being obtained from a single matrix diagonalization. So one of the cost advantages of wave functions over Green functions is not available in the present situation.

In the usual way the Green function G for the present problem is that which solves the *inhomogeneous* Schrödinger equation corresponding to Eq. (6). Expanding $G(\boldsymbol{r},\boldsymbol{r}';E)$ in the basis set $\{\chi_\mu(\boldsymbol{r})\}$,

$$G(\boldsymbol{r},\boldsymbol{r}';E)=\sum_{\mu\mu'} g(E)_{\mu\mu'}\chi_\mu(\boldsymbol{r})\chi^*_{\mu'}(\boldsymbol{r}') \tag{7}$$

the Green function expansion coefficients may be shown to satisfy the matrix equation

$$\sum_{\mu''}\left[H_{\mu\mu''}+G_0^{-1}(E)_{\mu\mu''}-EO_{\mu\mu''}\right]g(E)_{\mu''\mu'}=\delta_{\mu\mu'}\,, \tag{8}$$

where contributions to the matrix elements from the Hamiltonian, embedding potential, and overlap terms are

$$H_{\mu\mu'}=\int_{\mathrm{I}} d^3\boldsymbol{r}\chi^*_\mu H\chi_{\mu'}+\frac{1}{2}\int_S d^2\boldsymbol{r}_S\chi^*_\mu\frac{\partial}{\partial n_S}\chi_{\mu'}\,,$$

$$G_0^{-1}(E)_{\mu\mu'}=\int_S d^2\boldsymbol{r}_S\int_S d^2\boldsymbol{r}'_S\chi^*_\mu G_0^{-1}(E)\chi_{\mu'}\,, \tag{9}$$

$$O_{\mu\mu'}=\int_I d^3\boldsymbol{r}\chi^*_\mu\chi_{\mu'}\,.$$

We emphasize that the theory developed so far does not introduce any additional approximation beyond the single-particle model. In the usual manner Eq. (8) is solved self-consistently following the density functional theory in local density approximation,[26] as used here, or if desired by using gradient-corrected extensions to the LDA.[27] In this case $H=T+V_{\mathrm{eff}}(\boldsymbol{r})$ where T is the kinetic energy operator and

$$V_{\mathrm{eff}}(\boldsymbol{r})=V_{\mathrm{es}}(\boldsymbol{r})+V_{\mathrm{xc}}(\boldsymbol{r}) \tag{10}$$

is a sum of the electrostatic V_{es} and exchange-correlation V_{xc} potentials. Note that

$$V_{\mathrm{es}}(\boldsymbol{r})=\int d^3\boldsymbol{r}'\frac{\rho^+(\boldsymbol{r}')+\rho^-(\boldsymbol{r}')}{|\boldsymbol{r}'-\boldsymbol{r}|}, \tag{11}$$

where $\rho^++\rho^-$ contain the electronic charge plus the positive metallic charge and the nuclear one of the adparticle.

In practice, further approximations occur in the solution due to truncation of the basis set at a finite basis set size, introducing an error that can be monitored and in principle systematically reduced to any arbitrary level of precision required, and through the choice of embedding volume within which the solution is obtained self-consistently. In principle this too can be systematically increased and the error reduced to any desirable level.

C. Basis set and matrix elements

Differently from our previous work studing a noble-gas atom on a metal, where the effects of the core electrons (e.g., for Ne) were taken into account by using pseudopotentials, here we perform an all-electron calculation. This represents an improvement because interesting properties such as core-level shifts can be analyzed. For example the dependence of all valence and core electrons of He and Ne will be discussed in Sec. III. From the computational point of view a full potential calculation within the linearized augmented plane waves (FLAPW) method displays some advantages with respect to that performed in a pseudopotential framework with plane waves. They mainly refer to the treatment of atoms such Ne with a very deep pseudopotential that requires a much larger number of plane waves than of LAPW. So it is convenient to briefly discuss how we have adapted the LAPW method to our problem.

We recall first that the embedding approach is flexible enough to allow for an arbitrary basis set. For the present study, in which a single particle interacting with a surface is considered, a suitable generalization of the LAPW (Refs. 23 and 28) is an obvious choice. Note that we shall consider an all-electron description of a gas atom on jellium. The use of jellium has been justified in Sec. I, but we wish to stress that our treatment could be applied to a lattice structure too. Research is in progress in this direction. Also observe that for our problem the most suitable embedding region is a sphere of radius r_S centered on the adatom and including that portion of jellium significantly perturbed by the gas atom.

The idea of augmentation was first introduced in the augmented plane-wave basis.[29] Since the wave function varies rapidly inside the atomic core, an enormous number of plane waves is needed to describe this behavior in terms of plane waves only. Thus the idea of augmentation is to use different basis functions inside the atom (muffin-tin region), matching these augmentation functions to plane-wave basis functions outside a certain radius (r_{MT}). For a spherical region such as our embedding one, we use the following basis set

$$\chi_\mu(\boldsymbol{r})=\chi_{ilm}(r,\theta,\varphi)=\begin{cases}[A_l(k_i)u_l(r)+B_l(k_i)\dot{u}_l(r)]Y_L(\Omega) & \text{for } |\boldsymbol{r}|<r_{\mathrm{MT}}\\ j_l(k_ir)Y_L(\Omega) & \text{for } |\boldsymbol{r}|>r_{\mathrm{MT}}.\end{cases} \tag{12}$$

Note that to identify the above basis set, we adopt the commonly used acronym LAPW, though ours are linear augmented spherical (not plane) waves. The composite index μ represents both radial, i, and angular, $L=(l,m)$, indices. The functions $u_l(r)$ are the solutions of the radial atomic Schrödinger equation at a certain energy E_l, and $\dot{u}_l(r)$ are the energy derivatives of those solutions at E_l. This leads to an energy-independent LAPW, with an energy-linearized solution of the atomic Schrödinger equation. Explicitly for a pivot energy E_l, $u_l(r)$ and $\dot{u}_l(r)$ satisfy the following equations, respectively:

$$\begin{aligned}Hu_l(r)&=E_lu_l(r),\\ H\dot{u}_l(r)&=E_l\dot{u}_l(r)+u_l(r).\end{aligned} \tag{13}$$

The parameters $A_l(k_i)$ and $B_l(k_i)$ are used to match the augmentation function to the Bessel function j_l outside the muffin-tin region. In such a way the basis functions in Eq. (12) are continuous with continuous derivative at the muffin-tin radius. The values of the parameters $A_l(k_i)$ and $B_l(k_i)$ are

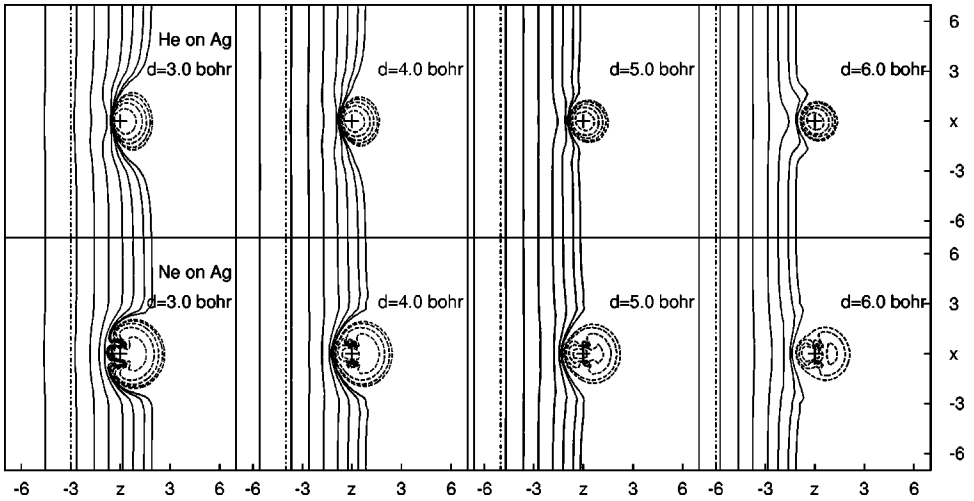

FIG. 2. Upper side: total charge density of a He atom interacting with an Ag-like jellium surface minus that of the free atom. The four horizontal panels refer to different distances d of He from the jellium edge (vertical dot-dashed line). Maps are plotted in the plane normal to the surface containing the atom nucleus. The normal direction is z. Contour values shown are 0.008, 0.003, 0.0012, ± 0.0005, ± 0.0002, ± 0.0001, ± 0.00005, ± 0.00003 electrons/a_0^3 (the solid line is positive, the dashed line is negative). Lower side: the same for a Ne atom.

$$A_l(k_i)=\frac{\dot{u}_l'(r_{\rm MT})j_l(k_i r_{\rm MT})-k_i j_l'(k_i r_{\rm MT})\dot{u}_l(r_{\rm MT})}{u_l(r_{\rm MT})\dot{u}_l'(r_{\rm MT})-\dot{u}_l(r_{\rm MT})u_l'(r_{\rm MT})},$$

$$B_l(k_i)=\frac{u_l(r_{\rm MT})k_i j_l'(k_i r_{\rm MT})-j_l(k_i r_{\rm MT})u_l'(r_{\rm MT})}{u_l(r_{\rm MT})\dot{u}_l'(r_{\rm MT})-\dot{u}_l(r_{\rm MT})u_l'(r_{\rm MT})}. \quad (14)$$

In the Bessel function argument, $k_n=n\pi/\tilde{a}$, where $\tilde{a}>r_S$, r_S being the radius of the embedding volume. This gives a range of values of amplitude and derivatives on the surface of the sphere and so does not prejudice or constrain the description of the boundary conditions. The matrix elements in Eqs. (8) and (9) on our LAPW basis set are defined in the Appendix.

III. RESULTS FOR He AND Ne ON Ag

In our calculations we use an embedding region of radius $r_S=7a_0$, while $r_{\rm MT}=2.8a_0$. We use the exchange-correlation functional in Ref. 30. Convergence is reached for an expansion with spherical waves with $l_{\max}=8$ and $i_{\max}=9$ radial components. The total charge densities of the interacting atom-Ag system either minus that of the He free atom or minus that of the Ne free atom, are displayed in Fig. 2. Figure 2 clearly visualizes the perturbation induced by the atom on the metal charge, showing that the atom acts as a pseudopotential that is essentially repulsive, pushing away the metal charge at shorter atom-metal distances d, while becoming more attractive at larger ones.[31] This repulsive feature at small d was also found previously.[13,19] In Fig. 2 note also a characteristic physisorption behavior with no intermingling of the atom and metal charges. The variation of the atom eigenenergies as a function of d together with the bare metal electrostatic potential $V_{\rm es}$ [see Eq. (11)] and the bare metal effective potential $V_{\rm eff}$ [see Eq. (10)], as a function of d, are given in Fig. 3 for the $1s$ level of He and in Fig. 4 for the $1s$, $2s$, and $2p$ of Ne. We shift all curves in energy so that their zero value is located at the largest d.[32] Our results show that far from the surface the level shifts follow the

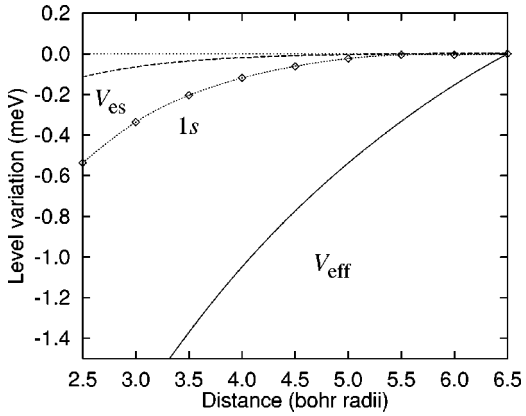

FIG. 3. The variations of the $1s$ level (line with diamonds) of a He atom, of the bare metal electrostatic potential $V_{\rm es}$ (dashed line), and of the bare metal effective potential $V_{\rm eff}$ (solid line) as functions of the atom jellium edge distance.

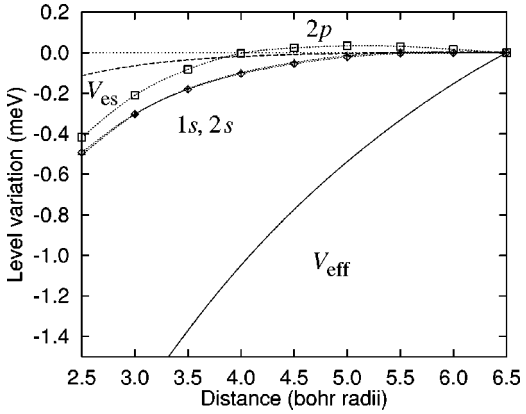

FIG. 4. The variations of the $1s$ (line with diamonds), $2s$ (line with crosses) and $2p$ (line with squares) levels of a Ne atom, of the bare metal electrostatic potential $V_{\rm es}$ (dashed line), and of the bare metal effective potential $V_{\rm eff}$ (solid line) as functions of the atom jellium edge distance.

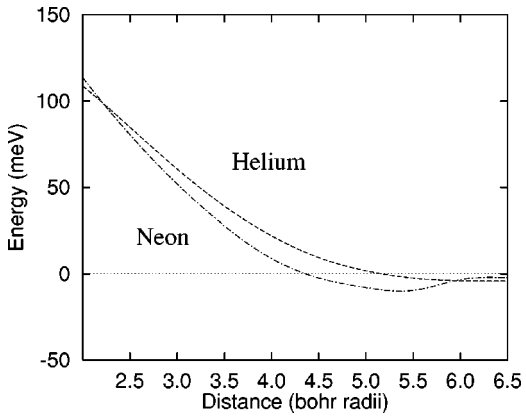

FIG. 5. The potential energies (meV) for a He (dashed line) and a Ne (dot-dashed line) atom, respectively, impinging on an Ag-like jellium surface as a function of the atom jellium edge distance.

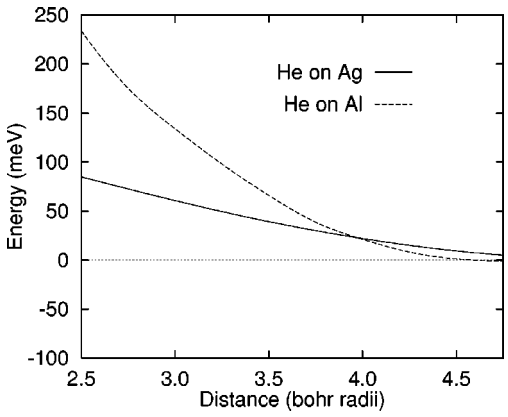

FIG. 6. The potential energies (meV) for a He atom impinging on an Ag-like (solid line) and on an Al-like (dashed line) jellium surface, respectively, as a function of the atom jellium edge distance.

variation of $V_{\rm es}$, while at shorter d they tend to follow the variation of $V_{\rm eff}$. This behavior could be explained by observing that at first order the shift $\delta\varepsilon_i$ of the eigenenergy ε_i is proportional to the variation of $V_{\rm eff}$, namely,

$$\delta\varepsilon_i(d) = V_{\rm eff}[\rho^{MA}] - V_{\rm eff}[\rho^A] \approx V_{\rm es}[\rho^M] + V_{\rm xc}[\rho^M + \rho^A] - V_{\rm xc}[\rho^A]. \quad (15)$$

In the expectation value in Eq. (15) the arguments ρ^{MA}, ρ^M, ρ^A are the atom-metal and the unperturbed metal and atom charge densities, respectively. When $\rho^A \gg \rho^M$, e.g., at large d, $\delta\varepsilon_i \approx V_{\rm es}[\rho^M]$, while at $\rho^A \ll \rho^M$, $\delta\varepsilon_i \approx V_{\rm eff}[\rho^M]$. As the atom approaches the metal surface, it experiences an increasing metal charge density, so that the limiting condition $\rho^A \gg \rho^M$ is no longer valid. A second effect, which at smaller d might raise $\delta\varepsilon_i(d)$ of the orbitals concentrated near the nucleus, is the charge transfer from the metal into the outer shell levels of the adatom. Such an effect, which is significant in previous calculations of chemisorbed adatoms (O, Cl, Si, Na) on Al,[32] is absent in physisorption, where the atoms are also much further away from the metal. Since, as to be discussed in the following, we shall present also the atom-metal potential energy (PES) of He and Ne, we add a comment on the comparison between the PES and $\delta\varepsilon_i$. In particular, we see from Fig. 4 that the $2p$ eigenvalue of Ne, differently from the $1s$ and $2s$, displays a maximum at about the same d where the PES has its minimum. The corresponding results for the $1s$ eigenvalue of He, whose energy is comparable to that of the $2p$ eigenvalue of Ne, do not contradict the previous behavior.

We now consider the energy dependence of the atom-metal potential $E(d)$ at various distances d from the jellium edge, calculated in the grand-canonical framework. Note that the outermost plane of substrate nuclei lies half an interplanar spacing behind the positive background edge (from 1.4 bohr to 2.2 bohr for different faces (110 or 100 or 111) of the metal surface). Figure 5 shows the PES's for He and Ne on Ag, respectively. Though at large enough atom-surface distances such curves require the contribution of the van der Waals tail not described in the LDA approach, for atom-surface repulsive potentials at smaller d, our results accurately describe the PES in the region relevant to noble-gas atom–metal elastic scattering experiments.[13]

An important result is that Ne is shown to penetrate deeper into the Ag electronic cloud than He for incoming particle energies up to about $E_{\rm cross} = 100$ meV,[34] where the two potential energy curves for He and Ne cross. The same result was already found on Al, but in this case $E_{\rm cross} = 240$ meV.[19] To explain these results, observe that the exchange-correlation contribution is larger for Ne than for He. This gives a somewhat more attractive character to Ne than to He in the repulsive potential region just discussed. Above the crossing point $E_{\rm cross}$, the Pauli repulsion dominates and the classical turning point becomes higher for Ne than for He at the same incident atom kinetic energies. It is also natural to compare our PES for He with that calculated by Lang and Norskøv[13] (LN) on the same Ag-like jellium in the same DFT framework. Such an analysis shows that from $E(d) \geqslant 30$ meV there is excellent agreement between the two calculations, though ours is performed with a different expansion, the LAPW, than that of LN. In the attractive region our minimum, which is as deep as that of LN, is shifted about $1a_0$ further from the metal. This is because our exchange-correlation expression[30] differs from that in LN, and gives a more attractive exchange-correlation hole energy, which is the one that is more relevant at larger d. We also observe very good agreement between our PES's and the PES's for He and Ne on Ag of Chizmeshya and Zaremba,[10] without the long-range correction. Note that the depth of the physisorption minimum of Ne on Ag is in good agreement with the results in Ref. 33. A comparison also between our results and those computed by a phenomenological method for He on Ag(100) and Ag(110) (Ref. 7) shows that the minimum of the physisorption potential is about the same.

We wish to point out that the results for He and Ne on Ag ($r_s^{\rm Ag} = 3.02a_0$) in this paper and our previous ones on Al-like jellium with higher density ($r_s^{\rm Al} = 2.07a_0$) display interesting differences. From Figs. 6 and 7, we observe the much smoother increase of the PES's of He and Ne on Ag. Also we observe that He and Ne atoms with the same impinging $E_{\rm kin}$ energy get closer to Al than to Ag up to about $E_{\rm kin} = 25$ meV for He and $E_{\rm kin} = 50$ meV for Ne, respectively. For larger energies the Al repulsion is much stronger. Such results can be accounted for, if we recall that an Al-like

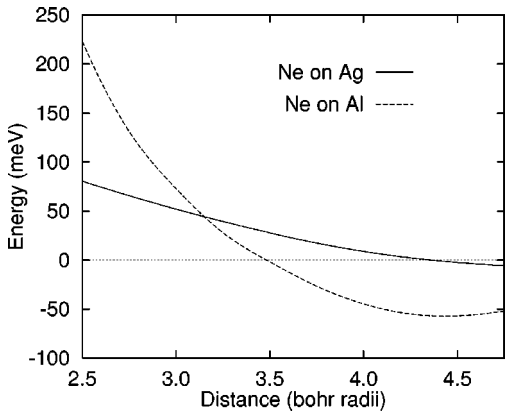

FIG. 7. The same as Fig. 6 but for a Ne atom.

jellium displays a larger electronic charge tail than that of a lower density metal such as Ag. For this reason, when either the Pauli repulsion (small d) or the attractive exchange-correlation (large d) effects dominate, the PES's of the noble-gas atom on the metal with greater density are either more repulsive or more attractive.

IV. CONCLUSIONS

The first contribution of this paper is the development of an all electron full potential calculation for an isolated adsorbate in the framework of the embedding method and of the DFT-LDA. This allows one to describe the variation of the core-level eigenvalues on the atom-surface separation not treated in previous work of He and Ne on metals. To deal with this problem we have applied the FLAPW basis set discussed in Sec. II C. This approach is also the most convenient to describe Ne and other adatoms, such as N, C, which display a deep pseudopotential.

The second result refers to the adiabatic atom-surface potential of light physisorbed noble gas atoms on Ag. Our results indicate that in the atom-surface range characteristic of noble-gas–surface scattering experiments, the turning point of He is farther from the surface than that of Ne. This is similar to the case of an Al substrate, and in agreement with experiments. We have also discussed the relevance of the substrate charge density on the dependence of the atom surface potential on the atom-metal distance.

ACKNOWLEDGMENTS

We are grateful to J.B.A.N. van Hoof for interesting discussions about the LAPW method and its implementation, and to S. Crampin for a careful reading of the manuscript.

APPENDIX: MATRIX ELEMENTS

The matrix elements of the different terms defined in Eq. (9) with respect to the LAPW basis are calculated as follows.

1. Overlap matrix elements

The overlap matrix in the muffin-tin region ($|\boldsymbol{r}|<r_{\mathrm{MT}}$) is

$$O^{\mathrm{MT}}_{\mu\mu'}=\int_{\mathrm{MT}} d^3\boldsymbol{r}\chi^*_{\mu}(\boldsymbol{r})\chi_{\mu'}(\boldsymbol{r})=\delta_{LL'}\left[A_l(k_i)A_l(k_j)+B_l(k_i)B_l(k_j)\int_0^{r_{\mathrm{MT}}} dr r^2[\dot{u}_{l'}(r)]^2\right], \tag{A1}$$

and in the interstitial region ($r_{\mathrm{MT}}<|\boldsymbol{r}|<r_S$):

$$O^{\mathrm{int}}_{\mu\mu'}=\int_{\mathrm{int}} d^3\boldsymbol{r}\chi^*_{\mu}(\boldsymbol{r})\chi_{\mu'}(\boldsymbol{r})=\delta_{LL'}\begin{cases} J^l_{k_i}(r_S)-J^l_{k_i}(r_{MT}) & \text{for } i=j \\ I^l_{k_i,k_j}(r_S)-I^l_{k_i,k_j}(r_{MT}) & \text{for } i\neq j \end{cases} \tag{A2}$$

with

$$I^l_{\alpha,\beta}(x)=\int_0^x dr r^2 j_l(\alpha r)j_l(\beta r)=\frac{x^2}{\alpha^2-\beta^2}[\beta j_l(\alpha x)j_{l-1}(\beta x)-\alpha j_{l-1}(\alpha x)j_l(\beta x)], \tag{A3}$$

$$J^l_{\alpha}(x)=\int_0^x dr r^2[j_l(\alpha r)]^2=\frac{x^3}{2}[j_l^2(\alpha x)-j_{l-1}(\alpha x)j_{l+1}(\alpha x)]. \tag{A4}$$

2. Hamiltonian matrix elements

To simplify the derivation we break up the expression for the Hamiltonian matrix element into several contributions. We start with the muffin tin, and a simple spherical potential, and then consider nonspherical contributions inside the muffin tin.

a. Spherical part. The Hamiltonian matrix element is

$$H^{\mathrm{MT}}_{\mu\mu'}=\int_{\mathrm{MT}} d^3\boldsymbol{r}\chi^*_{\mu}(\boldsymbol{r})(H+\Delta H)\chi_{\mu'}(\boldsymbol{r}), \tag{A5}$$

where H is the spherical part of the Hamiltonian and ΔH the nonspherical contribution. The spherical part can be written as

$$\int_{\mathrm{MT}} d^3\boldsymbol{r}\chi^*_{ilm}(\boldsymbol{r})H\chi_{jl'm'}(\boldsymbol{r}) = \int_{\mathrm{MT}} d^3\boldsymbol{r}[A_l(k_i)u_l(r)+B_l(k_i)\dot{u}_l(r)]^*Y^*_L(\Omega)H[A_{l'}(k_j)u_{l'}(r)+B_{l'}(k_j)\dot{u}_{l'}(r)]Y_{L'}(\Omega)$$
$$= \int_{4\pi} d\Omega Y^*_L(\Omega)Y_{L'}(\Omega)\int_0^{r_{\mathrm{MT}}} drr^2[A_l(k_i)u_l(r)+B_l(k_i)\dot{u}_l(r)]H[A_{l'}(k_j)u_{l'}(r)+B_{l'}(k_j)\dot{u}_{l'}(r)]$$
$$= \delta_{LL'}\Bigg[A_l(k_i)A_{l'}(k_j)\int_0^{r_{\mathrm{MT}}} drr^2u_l(r)Hu_{l'}(r)+A_l(k_i)B_{l'}(k_j)\int_0^{r_{\mathrm{MT}}} drr^2u_l(r)H\dot{u}_{l'}(r)$$
$$+B_l(k_i)A_{l'}(k_j)\int_0^{r_{\mathrm{MT}}} drr^2\dot{u}_l(r)Hu_{l'}(r)+B_l(k_i)B_{l'}(k_j)\int_0^{r_{\mathrm{MT}}} drr^2\dot{u}_l(r)H\dot{u}_{l'}(r)\Bigg]. \quad \text{(A6)}$$

Using Eq. (13), all the above integrals can be reduced to the numerical calculation of only three terms: $\langle\dot{u}_l|\dot{u}_l\rangle$, $\langle u_l|V|u_l\rangle$, and $\langle\dot{u}_l|V|u_l\rangle$.

b. Nonspherical part. In general the potential in the muffin tin is not spherically symmetric. This is especially true for an atom at a surface, where a spherically symmetric potential would provide a rather bad description. We use the general expansion of the potential in the muffin tin as given by

$$\Delta H = \sum_{L''}^{\tilde{n}_l} V^{\mathrm{eff}}_{L''}(r)Y_{L''}(\Omega). \quad \text{(A7)}$$

With calculations similar to that in Eq. (A6), we obtain

$$\Delta H^{\mathrm{MT}}_{\mu\mu'} = \int_{\mathrm{MT}} d^3\boldsymbol{r}\chi^*_{ilm}(\boldsymbol{r})\left[\sum_{L''}^{\tilde{n}_l} V^{\mathrm{eff}}_{L''}(r)Y_{L''}(\Omega)\right]\chi_{jl'm'}(\boldsymbol{r})$$
$$= \int_{\mathrm{MT}} d^3\boldsymbol{r}[A_l(k_i)u_l(r)+B_l(k_i)\dot{u}_l(r)]^*Y^*_L(\Omega)\left[\sum_{L''}^{\tilde{n}_l} V^{\mathrm{eff}}_{L''}(r)Y_{L''}(\Omega)\right][A_{l'}(k_j)u_{l'}(r)+B_{l'}(k_j)\dot{u}_{l'}(r)]Y_{L'}(\Omega)$$
$$= \sum_{L''}^{\tilde{n}_l}\left[\int_{4\pi} d\Omega\ \ Y^*_L(\Omega)Y_{L''}(\Omega)Y_{L'}(\Omega)\right]\int_0^{r_{\mathrm{MT}}} drr^2[A_l(k_i)u_l(r)+B_l(k_i)\dot{u}_l(r)]V^{\mathrm{eff}}_{L''}(r)[A_{l'}(k_j)u_{l'}(r)+B_{l'}(k_j)\dot{u}_{l'}(r)]$$
$$= \sum_{L''}^{\tilde{n}_l} O_{LL''L'}\int_0^{r_{\mathrm{MT}}} drr^2[A_l(k_i)u_l(r)+B_l(k_i)\dot{u}_l(r)]V^{\mathrm{eff}}_{L''}(r)[A_{l'}(k_j)u_{l'}(r)+B_{l'}(k_j)\dot{u}_{l'}(r)], \quad \text{(A8)}$$

where $O_{LL''L'}=\int_{4\pi}d\Omega\ \ Y^*_L(\Omega)Y_{L''}(\Omega)Y_{L'}(\Omega)$. The four kinds of integrals in Eq. (A8) have to be evaluated numerically.

Now we handle the Hamiltonian matrix elements in the interstitial region. In this case the basis functions are simply Bessel functions and consequently all terms are easier to compute than in the muffin tin. In the interstitial region the normal derivative and the embedding potential also have to be considered [see Eq. (6) and following].

The kinetic energy is straightforward, as the basis functions are eigenstates of the kinetic energy operator with eigenvalue $k_i^2/2$:

$$T^{\mathrm{int}}_{\mu\mu'} = \frac{k_j^2}{2}O^{\mathrm{int}}_{\mu\mu'}. \quad \text{(A9)}$$

The normal derivative is

$$D_{\mu\mu'} = \delta_{LL'}\frac{r_S}{2}j_l(k_ir_S)[lj_l(k_jr_S)-k_jr_Sj_{l+1}(k_jr_S)], \quad \text{(A10)}$$

making use of recurrence relations satisfied by the Bessel functions.[35]

The potential is expanded as in Eq. (A7). The radial components $V_L(r)$ are tabulated on a grid and include contributions from the ionic core, known analytically, the Coulomb contribution, which is found from the solution of the Poisson equation (this reduces to the solution of a radial problem for each L component), and the exchange-correlation potential, which is numerically evaluated by fitting its angular variation via a special directions expantion.

The contribution to the Hamiltonian matrix elements from the potential is

$$V^{\mathrm{int}}_{\mu\mu'} = \sum_{L''} O_{LL'L''}\int_{r_{MT}}^{r_S} drr^2j_l(k_ir)V_{L''}(r)j_{l'}(k_jr). \quad \text{(A11)}$$

Finally, the matrix elements of the embedding potential are

$$G_0^{-1}(E)_{\mu\mu'} = r_S^4\mathcal{G}_0^{-1}(E)_{LL'}j_l(k_ir_S)j_{l'}(k_jr_S), \quad \text{(A12)}$$

where $\mathcal{G}_0^{-1}(E)_{LL'}$ are the expansion coefficient of $G_0^{-1}(\boldsymbol{r}_S,\boldsymbol{r}'_S,E)$ onto the spherical harmonics.

[1] E. Hult, Y. Andersson, B. I. Lundqvist, and D. C. Langreth, Phys. Rev. Lett. **77**, 2029 (1996); E. Hult and A. Kiejna, Surf. Sci. **383**, 88 (1997).
[2] M. Karikorpi, M. Manninen, and C. Umrigar, Surf. Sci. **169**, 299 (1986).
[3] G. P. Brivio and T. B. Grimley, Surf. Sci. Rep. **17**, 1 (1993).
[4] Y. Takada and W. Kohn, Phys. Rev. Lett. **54**, 470 (1985).
[5] E. C. Goldberg, A. Martín-Rodero, R. Monreal, and F. Flores, Phys. Rev. B **39**, 5684 (1989).
[6] K. Lenarcic-Poljanec, M. Hodoscek, D. Lovrić, and B. Gumhalter, Surf. Sci. **251/252**, 706 (1991).
[7] K. T. Tang and J.P. Toennies, Surf. Sci. Lett. **279**, L203 (1992).
[8] J. Ellis, K. Hermann, F. Hofmann, and J. P. Toennies, Phys. Rev. Lett. **75**, 886 (1995).
[9] J. Harris and A. Liebsch, J. Phys. C **15**, 2275 (1982).
[10] A. Chizmeshya and E. Zaremba, Surf. Sci. **268**, 432 (1992).
[11] W. Kohn, in *Interaction of Atoms and Molecules with Solid Surfaces*, edited by V. Bortolani, N. H. March, and N. P. Tosi (Plenum, New York, 1990), p. 53.
[12] N. D. Lang, Phys. Rev. Lett. **46**, 842 (1981).
[13] N. D. Lang and J. K. Nørskov, Phys. Rev. B **27**, 4612 (1983).
[14] M. I. Trioni, G. P. Brivio, S. Crampin, and J. E. Inglesfield, Phys. Rev. B **53**, 8052 (1996).
[15] D. M. Bird and P. A. Gravil, Surf. Sci. **377-379**, 555 (1997).
[16] We use here and throughout the paper atomic units: $c=e=\hbar=m_e=1$. So lengths will be in bohr radii a_0 and energies in Hartree, unless otherwise stated.
[17] E. Zaremba and W. Kohn, Phys. Rev. B **13**, 2270 (1976); **15**, 1769 (1977).
[18] M. Petersen, S. Wilke, P. Ruggerone, B. Kohler, and M. Scheffler, Phys. Rev. Lett. **76**, 995 (1996).
[19] F. Montalenti, M. I. Trioni, G. P. Brivio, and S. Crampin, Surf. Sci. Lett. **364**, L595 (1996).
[20] M. I. Trioni, F. Montalenti, and G. P. Brivio, Surf. Sci. Lett. **401**, L383 (1998).
[21] J. E. Inglesfield, J. Phys. C **14**, 3795 (1981).
[22] G. A. Benesh and J. E. Inglesfield, J. Phys. C **17**, 1595 (1984).
[23] J. E. Inglesfield and G. A. Benesh, Phys. Rev. B **37**, 6682 (1988).
[24] P. Hohenberg and W. Kohn, Phys. Rev. **136**, B864 (1964); W. Kohn and L. J. Sham, Phys. Rev. **140**, A1133 (1965).
[25] B. Drittler, M. Weinert, R. Zeller, and P. H. Dederichs, Phys. Rev. B **39**, 930 (1989).
[26] S. Lundqvist and N. H. March, *Theory of the Inhomogeneous Electron Gas* (Plenum Press, New York, 1983).
[27] J. P. Perdew, in *Electronic Structure of Solids*, edited by P. Ziesche and H. Eschrig (Akademie Verlag, Berlin, 1991).
[28] P. W. Anderson, Phys. Rev. **124**, 41 (1961); O. K. Andersen, Phys. Rev. B **12**, 3060 (1975).
[29] J. C. Slater, Phys. Rev. **51**, 846 (1937).
[30] D. M. Ceperley and B. J. Alder, Phys. Rev. Lett. **45**, 566 (1980).
[31] J. E. Inglesfield and J. P. Perdew, Philos. Mag. **34**, 205 (1976).
[32] N. D. Lang and A. R. Williams, Phys. Rev. B **18**, 616 (1978).
[33] S. Ossicini, Phys. Rev. B **33**, 873 (1986).
[34] M. G. Dondi, C. Mannori, D. Cvetko, L. Floreano, A. Morgante, M. Peloi, and F. Tommasini, Surf. Sci. **377-379**, 710 (1997).
[35] G. Arfken, *Mathematical Methods for Physicists* (Academic Press, New York, 1985).